nature chemistry

ARTICLES

https://doi.org/10.1038/s41557-018-0127-3

A fluorescent membrane tension probe

Adai Colom[1,2,3], Emmanuel Derivery[1,2,3,4], Saeideh Soleimanpour[2,3], Caterina Tomba[1,3], Marta Dal Molin[2,3], Naomi Sakai[2,3], Marcos González-Gaitán[1,2,3], Stefan Matile[2,3] and Aurélien Roux[1,2,3]*

Cells and organelles are delimited by lipid bilayers in which high deformability is essential to many cell processes, including motility, endocytosis and cell division. Membrane tension is therefore a major regulator of the cell processes that remodel membranes, albeit one that is very hard to measure in vivo. Here we show that a planarizable push–pull fluorescent probe called FliptR (fluorescent lipid tension reporter) can monitor changes in membrane tension by changing its fluorescence lifetime as a function of the twist between its fluorescent groups. The fluorescence lifetime depends linearly on membrane tension within cells, enabling an easy quantification of membrane tension by fluorescence lifetime imaging microscopy. We further show, using model membranes, that this linear dependency between lifetime of the probe and membrane tension relies on a membrane-tension-dependent lipid phase separation. We also provide calibration curves that enable accurate measurement of membrane tension using fluorescence lifetime imaging microscopy.

Cells and organelles are delimited by lipid membranes. Membranes are fluid surfaces, ~4 nm thick, and are diffusion barriers to most solutes (but not to water). Membrane shape changes can cause bending, shearing and stretching, and membrane tension is defined as the derivative of the membrane free energy with area change[1,2]. Lipid membranes are very resistant to stretch, supporting tensions up to 10^{-2} N m^{-1} before lysis, with a few percent of area change[3,4].

Membrane tension plays an essential role in numerous cell processes. At the whole cell level, membrane tension is tightly regulated during cell migration[5–8], cell spreading and phagocytosis[9,10]. During cell division, membrane tension causes a volume instability between daughter cells that is counteracted by contraction of the actin cortex[11]. Increased tension delays the last step of cell division, abscission[12]. Membrane tension also regulates subcellular processes. For example, increased tension inhibits endocytosis[13] by counteracting clathrin polymerization[14] and activating membrane fission[15]. Membrane tension regulates the opening of mechanosensitive ion channels[16], and the activity of TORC2, a major regulator of cell metabolism[17]. As a consequence of its multiple roles, membrane tension is constantly regulated by the cell[18].

Despite its importance in the regulation of many cell processes, membrane tension remains notoriously difficult to measure in cells: so far, the only technique available is extraction of small membrane tubes from the plasma membrane[5,18,19]. Although this technique has provided valuable insights over the past decade, it suffers from several limitations. First, the tube radius and the force required to maintain the tube—measurements necessary for calculation of the tension—are complex to obtain independently[5]. Second, because formation of the tube requires peeling the membrane off the actin cortex, the adhesion energy of the membrane onto the actin cortex adds up to the membrane tension value. Finally, this technique cannot measure the tension of intracellular membranes such as organelles.

The importance of membrane tension in biological processes called for non-invasive fluorescent probes that would allow for its measurement in living cells. However, no existing tension probes have been shown to be reliable in living cells[20–30]. One approach, which is technically challenging, is to use the homo-FRET (Föster resonance energy transfer) signal of mechanosensitive ion channels[16]. Among the different mechanisms explored, photo-induced electron transfer is better for voltage sensitivity[26], whereas solvatochromism[21,28] and excited-state deplanarization in molecular rotors[23,24,28–31] are most promising for imaging membrane order.

Recently, we introduced complementary ground-state planarization as a new approach to mechanosensitive membrane probes[32]. Planarizable push–pull probes can report lipid packing changes through changes in their fluorescence parameters. Lipid packing is defined as the density of lipid acyl chains: higher lipid packing is reflected by tighter and more ordered acyl chains, and lower lipid packing corresponds to more spaced and disordered acyl chains. Thus, liquid-ordered phases have higher lipid packing than liquid-disordered phases. We showed that these planarizable push–pull probes can distinguish different phases with different order[33]. In more ordered phases, lipid packing is higher, as acyl chains apply a higher pressure that planarizes the push–pulled probes.

Membrane tension is also expected to change lipid packing by stretching the lipids away. However, the area increase from this stretching is very small, with a maximum of 8% before lysis[34]. Because our push–pull probes are extremely sensitive to lipid packing, we wondered if they could report such changes in membrane tension. Among the several push–pull probes we designed[2,32,33,35,36], we called the most promising probe for measuring membrane tension, **FliptR** (for 'fluorescent lipid tension reporter', Fig. 1a)[2].

FliptR consists of two large dithienothiophene flippers[33] (Fig. 1a). In a non-confining environment, the two flippers are twisted out of conjugation by repulsion between the methyls and the endocyclic sulfurs next to the connecting, rotatable bond. The negatively charged carboxylate in the headgroup[2] helps to assure oriented insertion into membranes. **FliptR** has high photostability[2], partitions almost equally into different membrane phases[33], has different fluorescence absorption/emission spectra between lipid phase[2], do not change position following a lipid phase transition[33], and does not disturb membrane order like, for example, cholesterol[36]. **FliptR** can planarize with an increase in lateral pressure (Fig. 1b). Here, we report that **FliptR** can be used to image a

[1]Biochemistry Department, University of Geneva, Geneva, Switzerland. [2]Swiss National Centre for Competence in Research Programme Chemical Biology, Geneva, Switzerland. [3]School of Chemistry and Biochemistry, University of Geneva, Geneva, Switzerland. [4]Present address: MRC Laboratory of Molecular Biology, Cambridge Biomedical Campus, Cambridge, UK. *e-mail: Aurelien.Roux@unige.ch

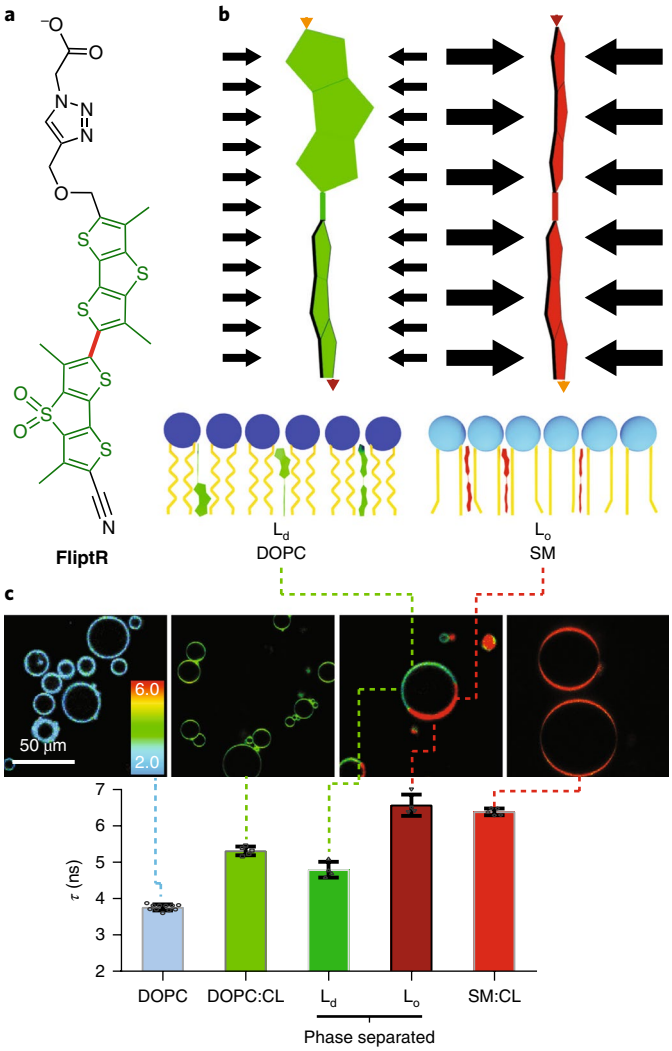

Fig. 1 | The FliptR probe. a, Chemical structure. The carbon bond around which the fluorescent groups (green) can twist is shown in red. **b**, Pressure along the axis of the **FliptR** probe can planarize the two fluorescent groups, leading to changes in excitation maxima and fluorescence lifetime (see main text). **c**, Fluorescence lifetime τ_1 images of **FliptR** as a function of lipid composition in giant unilamellar vesicles, from liquid-disordered membrane (L_d) to increasingly liquid-ordered membrane (L_o). Corresponding lifetime mean values are shown in the histogram. Compositions are 1,2-dioleoyl-*sn*-glycero-3-phosphocholine (DOPC) (N = 5, R = 15); DOPC:CL (cholesterol) 60:40 (N = 5, R = 25); phase-separated DOPC:sphingomyelin (SM):CL 25:58:17 (N = 4, R = 5); and SM:CL 70:30 (N = 5, R = 25). Mean ± s.d. The colour bar corresponds to lifetime in nanoseconds (ns).

combination of lipid composition and membrane tension in live cells and artificial membranes.

Results and discussion

FliptR reports lipid order in artificial membranes. With the aim of imaging membrane tension in living cells, the large change in **FliptR** fluorescence lifetime with lipid phase caught our interest, as it reflects a high sensitivity to lipid packing. Moreover, the fluorescence lifetime is independent of intensity, which changes by a factor of 10 in the planarized state versus the twisted state and is thus also independent of the optical set-up used to measure it.

We first studied if the fluorescence lifetime of the probe could report the ordering state of various lipid phases. We electroformed giant unilamellar vesicles (GUVs) of different compositions with 1 mol% **FliptR**, and imaged their lifetimes using fluorescence lifetime imaging microscopy (FLIM). The fluorescence emission decay curves were fitted with double exponentials, from which two lifetimes (τ_1 and τ_2) and two intensities (I_1 and I_2) could be extracted (see Methods). As for **FliptR**, the second component of the lifetime, τ_2, only accounts for a minority of the signal, with a low number of photons (I_2) (Supplementary Fig. 1a). Lifetime data presented in the following correspond to the longest component, τ_1. This is justified by the fact that τ_2 values are more subject to errors, as they are smaller and account for fewer emission events, and also because τ_1 is linked to the time taken for intramolecular charge transfer and thus reports directly on the mechanism by which **FliptR** senses applied forces.

The lifetime of **FliptR** increased with the proportion of lipids forming the liquid-ordered (L_o) phase. The **FliptR** fluorescence lifetime was 3.75 ± 0.08 ns (mean ± s.d., as in the rest of the text, unless noted; $N = 11$, $R = 43$, Fig. 1c) for GUVs made only of 1,2-dioleoyl-*sn*-glycero-3-phosphocholine (DOPC), which forms the liquid-disordered phase (L_d) above 0 °C, 5.31 ± 0.12 ns ($N = 5$, $R = 15$, with N being the number of experiments and R the number of GUVs) for GUVs made of DOPC and cholesterol (CL) (DOPC:CL, 60:40) which increases lipid order, and 6.39 ± 0.09 ns ($N = 5$, $R = 25$) for GUVs composed of brain sphingomyelin (SM) and CL (70:30), forming a liquid-ordered phase. Moreover, when phase-separated GUVs were formed (DOPC:SM:CL 25:58:17), different domains could easily be imaged by measuring the **FliptR** lifetime (Fig. 1c, L_d and L_o). Interestingly, the lifetime of **FliptR** in one of the domains was close to that in DOPC:CL 60:40 membranes (4.79 ± 0.21 ns ($N = 4$, $R = 5$), compared to 5.31 ns for DOPC:CL 60:40), while the lifetime in the other domain was very close to the lifetime of GUVs made of SM and CL only (6.57 ± 0.29 ns ($N = 4$, $R = 5$) compared to 6.39 ns for SM:CL 70:30). These results show that **FliptR** is sensitive to lipid composition by detecting the various packing of lipids in different phases with different order (Fig. 1c)[2].

FliptR reports lipid order in cellular membranes. We then tested if **FliptR** could detect lipid composition and/or phase differences in living cells. We used HeLa fibroblastic cells and Madin–Darby canine kidney (MDCK) epithelial cells, and when micromolar amounts of **FliptR** were added to the medium of non-confluent HeLa and MDCK cells, plasma membrane staining appeared in less than one minute, with enough signal to measure the lifetime accurately (Fig. 2a and Supplementary Video 1). However, in epithelial cells, the apical membrane has been reported to form a large L_o domain due to enrichment in shingolipids and cholesterol, while the basolateral membrane is reported to form a less ordered lipid phase[37], in which **FliptR** required more time to reach the basolateral side (Supplementary Fig. 1b). This may be due to the diffusion barrier created by the tight junctions between the apical side (to which **FliptR** is delivered) and the basolateral side. **FliptR** remained stably in the plasma membrane, even though limited endosomal labelling appeared after two hours of incubation with **FliptR**, most probably due to endocytic recycling of the probe (Supplementary Fig. 1b). We did not notice any cell growth and/or viability defects in up to four days of culture in the presence of **FliptR** (Supplementary Fig. 1b).

In polarized confluent MDCK cells that have been grown on microstructured surfaces to provide different orientations of the cells towards the microscope, two clearly different lifetimes were observed (Fig. 2b). The lifetime on the apical side (towards the medium) is higher than on the basolateral (Fig. 2b, red colour on the apical side and green on the basolateral side), matching the lipid order difference in these two parts of the cells[37,38]. This finding clearly shows that **FliptR** also detects lipid packing differences in different parts and/or compartments of epithelial cells.

FliptR reports changes of osmotic pressure. We then wondered if **FliptR** could detect changes in membrane tension in cells. A com-

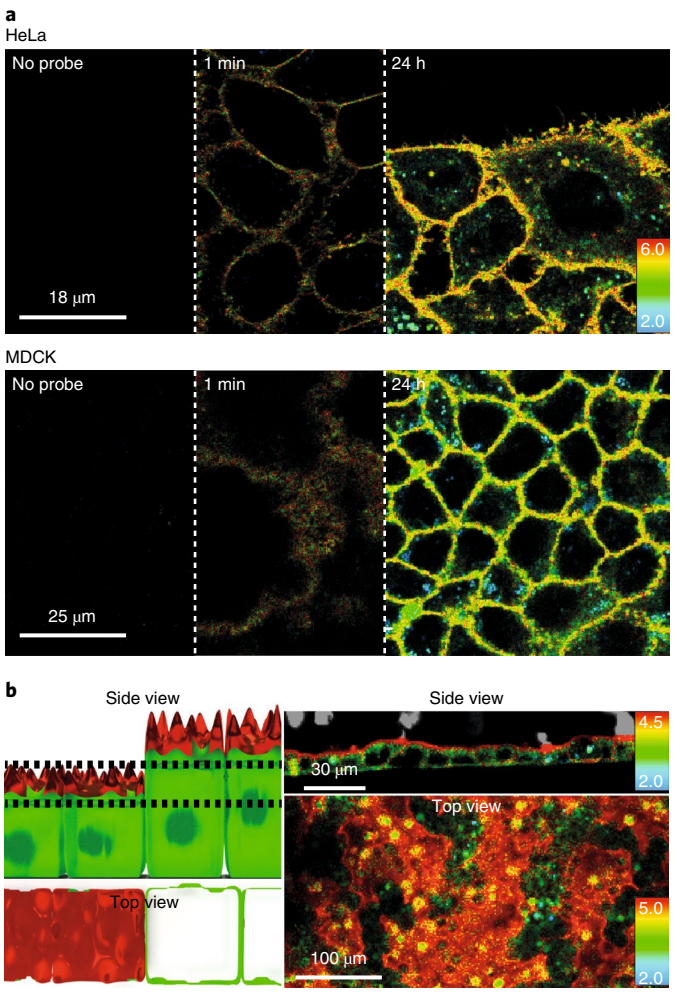

Fig. 2 | Different FliptR lifetimes correspond to different lipid compositions in cells. a, Labelling of MDCK and HeLa cells with time. **FliptR** mostly stays in the plasma membrane. However, after 2 h of incubation, bright spots with low lifetime values (more blue colours) are seen, probably corresponding to endosomes ($N = 4$). **b**, MDCK epithelial cells show longer lifetimes on the apical side (red on the side view) than on the basolateral part (green). The top view corresponds to a single confocal plane (between dashed lines in the left side view schematics), and, depending on the height of the cells, either the apical side (red) or the basolateral part (green) is visible ($N = 4$). The colour bar corresponds to lifetime in ns.

mon way to change the membrane tension of cells is to apply osmotic shocks. During hypoosmotic shocks (low osmotic pressure Π from the cell culture medium), the cell volume and plasma membrane tension increase[39,40]. In contrast, under hyperosmotic shock (high osmolarity Π), the volume and membrane tension decrease (Fig. 3a)[40,41]. When applying hypoosmotic shocks ($\Pi < 0.3$ Osm) on Hela and MDCK cells loaded with **FliptR**, we robustly observed longer lifetimes than in isoomostic conditions ($\Pi = 0.3$ Osm), but shorter under hyperosmotic shocks ($\Pi > 0.3$ Osm) (Fig. 3b). Whereas the **FliptR** fluorescence lifetime τ_1 stayed constant when cells were kept in isoosmotic conditions (Supplementary Fig. 2a), it changed rapidly after hypoosmotic and hyperosmotic shocks (Supplementary Fig. 2b). Overall, the dependence of τ_1 on osmotic pressure Π from the cell medium was linear for both HeLa and MDCK cells (Fig. 3b), but the slopes were clearly different (slope $= -0.52 \pm 0.03$ versus -0.84 ± 0.04 ns Osm^{-1}, respectively, mean $\pm$ s.e.). Moreover, a better fit was obtained by fitting hypoosmotic data independently of hyperosmotic data (Supplementary Fig. 2c). In this case, both for HeLa and MDCK cells, the slopes of the hypoosmotic data are about 0.3–0.4 ns Osm^{-1} less than for hyperosmotic data (Hela: Hypo, -0.27 ± 0.13 ns Osm^{-1} and Hyper: -0.59 ± 0.04 ns Osm^{-1}; MDCK: Hypo, -0.50 ± 0.33 ns Osm^{-1}, Hyper: -0.88 ± 0.07 ns Osm^{-1}, mean $\pm$ s.e.). This may be explained by lowering of lipid packing following a tension increase (see Fig. 4 and discussion).

To test the possibility that membrane-tension-dependent changes of the **FliptR** lifetime are not coupled to cell active processes such as cortical acto-myosin contraction or active ion pumping, osmotic shocks were applied to GUVs with a lipid composition mimicking the cell plasma membrane (POPC:SM:CL 57:14:29) and loaded with **FliptR** (Fig. 3a). We found that **FliptR** lifetime τ_1 also increased with hypoosmotic shocks, and decreased with hyperosmotic shocks, in a way similar to that in cells (Fig. 3b). Similarly, **FliptR** lifetime changed linearly with Π, although the changes were smaller (slope = –0.22 ns Osm^{-1}). The robust change of τ_1 in proportion to Π suggests that the lifetime of **FliptR** could monitor changes in plasma membrane tension.

FliptR reports membrane tension in cells. To measure membrane tension while applying osmotic shocks to the same cell, optical tweezers were used to pull away concanavalin A-coated polystyrene beads that had been previously attached to the cell membrane, to produce thin membrane tubes (Fig. 3c)[42]. The force required to hold the bead is a direct measure—although not absolute—of cell membrane tension. We calculated the membrane tension σ from the force data using a measured value of the cell membrane bending rigidity, typically 0.14 pN µm, corresponding to 35 k_BT (ref. [5]).

We then applied an osmotic shock by flushing a new solution into the microscopy chamber (see Methods) while recording **FliptR** lifetime and tube force. Hypoosmotic shocks led to a moderate increase in tube force, indicating a slight increase in membrane tension, whereas hyperosmotic shocks led to a dwindling of tube force, indicating a large membrane tension drop (Fig. 3d). The change in τ_1 was linear with membrane tension σ, increasing with increasing tension. For MDCK cells, the slope was 2.38 ± 0.18 ns m mN^{-1} until reaching saturation for tension values above 0.6 mN m^{-1}, and was 0.196 ± 0.07 ns m mN^{-1} after this limit (Fig. 3d). For HeLa cells, the dependence was similar; from 0 to 0.6 mN m^{-1} the slope was 0.78 ± 14 ns m mN^{-1}, then 0.26 ± 0.06 ns m mN^{-1} at higher tensions (Fig. 3d). Importantly, the change in slope (Fig. 3d) occurred for membrane tension values obtained under isoosmotic conditions. Values higher than the value of membrane tension in isotonic conditions were obtained for hypoosmotic shocks, whereas membrane tension values below isotonic conditions were obtained with hypertonic shock. Thus, the change in slope occurring under isotonic conditions may be due to an additional effect acting on **FliptR** under hypotonic conditions. As for lifetime as a function of osmotic pressure (Fig. 3b), this additional effect may be caused by a reduction in lipid packing (see Fig. 4 and discussion). These results clearly show that **FliptR** fluorescence lifetime reports membrane tension in cells, and that calibration is needed for each cell type.

FliptR response in single lipid phase membrane is the inverse of that in cells. The response of mechanosensitive flipper probe **FliptR** to changes in membrane tension in cells and GUVs (Fig. 3) could conceivably originate from several structural changes (Fig. 4). A change in lipid packing is perhaps the most intuitive outcome of membrane tension (Fig. 4a,b)[4,34,43]. However, increasing distances between lipid acyl chains following an increase in membrane tension should result in a more deplanarized state of **FliptR**. Increasing tension should thus lead to decreasing lifetimes, an opposite response to that observed in cells (Fig. 3).

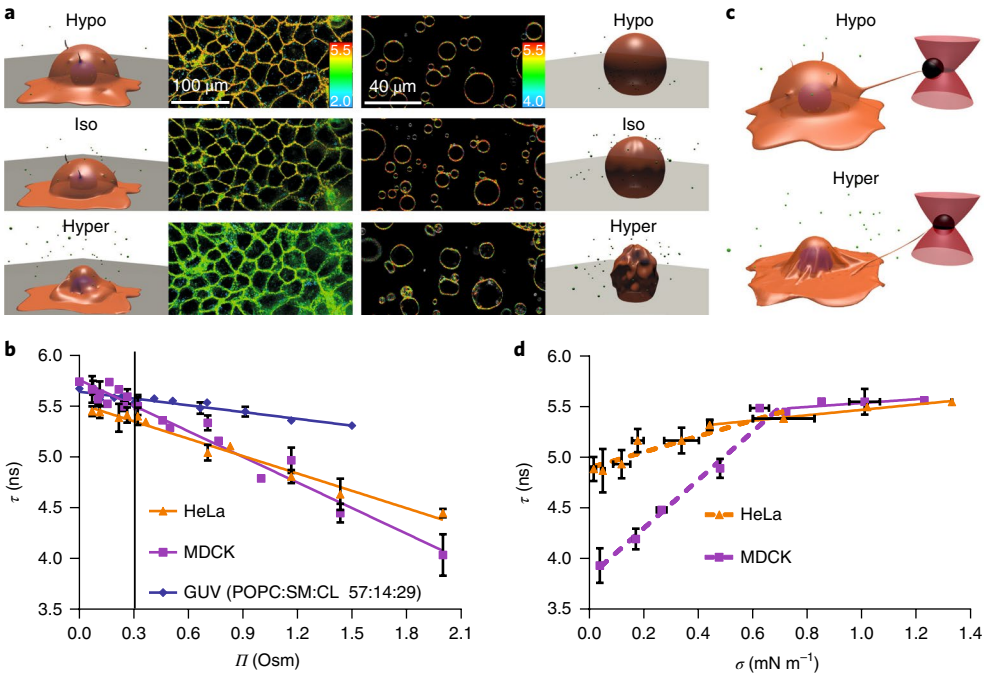

Fig. 3 | Response of FliptR fluorescence lifetime to osmotic shocks on cells and GUVs. a, FLIM images of MDCK and GUVs (POPC:SM:CL 57:14:29) in isoosmotic buffer, and after hyper- or hypoosmotic shocks. **b**, **FliptR** fluorescence lifetime τ_1 as a function of osmotic pressure Π applied to HeLa cells (orange triangles, slope hypo = −0.27 ± 0.13 ns Osm^{-1}, slope hyper = −0.59 ± 0.04 ns Osm^{-1}, mean ± s.d. as in the rest of the measurements, N = 20); MDCK cells (purple squares, slope hypo = −0.50 ± 0.33 ns Osm^{-1}, slope hyper = −0.88 ± 0.07 ns Osm^{-1}, N = 6); and GUVs (blue diamonds, slope hypo = −0.19 ± 0.18 ns Osm^{-1}, slope hyper = −0.22 ± 0.03 ns Osm^{-1}, N = 4), with linear curve fit. Black line represents the initial state. **c**, To correlate osmotic pressure Π with membrane tension σ, cells were connected to optical tweezers through pulled-out lipid nanotubes, and σ was calculated from the tube force measured in response to osmotic shocks applied. **d**, **FliptR** fluorescence lifetime τ_1 as a function of membrane tension σ applied by osmotic shocks to HeLa (orange triangles, slope hypo = 0.26 ± 0.06 ns m mN^{-1}, slope hyper = 0.78 ± 0.14 ns m mN^{-1}, N = 7) and MDCK cells (purple squares, slope hypo = 0.16 ± 0.07 ns m mN^{-1}, slope hyper = 2.38 ± 0.18 ns m mN^{-1}, N = 11) with pulled-out tubes connected to optical tweezers (**c**), with fits to the linear range before the onset of saturation above τ_1 = 5.5 ns. The colour bar corresponds to lifetime in ns.

We nevertheless carried on testing this hypothesis using SM:CL 70:30 GUVs, which consist of the L_o phase, thus with high lipid packing at low membrane tension, as reflected by the high **FliptR** lifetime values in these membranes (Fig. 1c). By aspirating these L_o GUVs labelled with 1 mol% **FliptR** with a micropipette, we controlled and changed their tension. This tension was measured by the extraction of small membrane tubes with optical tweezers (Fig. 5a,b). As expected from our hypothesis, L_o SM:CL 70:30 GUVs demonstrated a linear decrease in **FliptR** lifetime with increasing tension, with a slope = −1.32 ± 0.19 ns m mN^{-1} (Fig. 5b). Thus, in single-phase membranes, the **FliptR** response to tension is indeed dominated by loosened lipid packing with increasing distances between lipid tails (Fig. 4b). This effect could also be seen as a tension-induced lipid phase transition: tension may exert pulling forces on the acyl chains of lipids, allowing them to melt from the L_o into the L_d phase.

In membranes with a composition closer to plasma membrane (POPC:SM:CL 57:14:29), the decrease in **FliptR** lifetime in response to increasing tension was much less pronounced (Fig. 5b, slope = −0.27 ± 0.05 ns m mN^{-1}). Because of the pipette aspiration used in these experiments, only conditions where membrane tension increased could be tested (Fig. 3b). This suggested that even if the response of these GUVs to micropipette aspiration is dominated by loosened lipid packing, another molecular mechanism would lower the response of **FliptR** to increasing tension. Indeed, the small decrease in **FliptR** lifetime with increasing tension applied by micropipette aspiration (Fig. 5b) was contrary to the significant increase in **FliptR** lifetime with decreasing osmotic pressure (membrane tension increase) in cells and GUVs (Fig. 3b).

FliptR response to tension depends on lipid phase separation. We then studied the nature of this additional molecular mechanism. One of the possible explanations for the increasing **FliptR** lifetime with increasing tension is that lipid tails would tilt on increasing the surface area (Fig. 4c). Tilted lipid tails could be a way to adapt the rapid change of surface as observed in stretched polymer chemistry[44]. Also, tilted lipid tails are a characteristic feature of peculiar gel phases called L_β that accommodate tight packing with a surface increase[45]. Chain stretching and lipid tilting in response to increasing membrane tension would cause lateral compression of the acyl chains, leading to **FliptR** planarization and increasing its lifetime. This effect is expected to be independent of the lipid phase. We thus tested this tilting hypothesis in pure L_d GUVs composed of DOPC only, and subjected them to hypo- or hyperosmotic shocks, which did not change the lifetime of **FliptR** (Supplementary Fig. 3a). We thus concluded that the tilting was not the mechanism causing lifetime changes in response to tension changes in cells.

Planarizable push–pull probes have been suspected previously to be planarizable also by voltage because of macrodipole–potential interactions[32]. Cell membranes have a voltage potential created by the ionic gradients across them. Although experimental support for significant voltage sensitivity could not be obtained, possible contributions to the response of the **FliptR** probe to tension had to be tested. For this purpose, we loaded neurons (cells with high membrane potential) with **FliptR** and depolarized them with an isoosmotic buffer containing 47 mM KCl (see Methods). During KCl treatment, the **FliptR** lifetime did not change significantly (Supplementary Fig. 4). However, on adding a 700 mOsm hyperosmotic sucrose solution, the **FliptR** lifetime dropped significantly

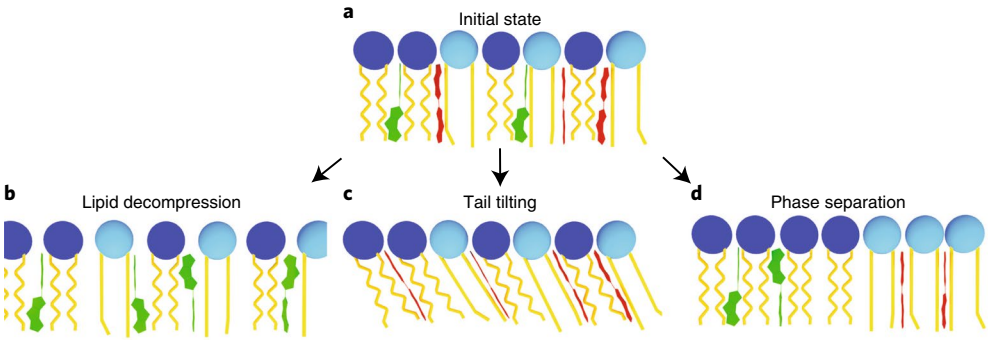

Fig. 4 | Possible structural changes of lipid bilayer membranes in response to tension reported by FliptR. a, Initial state where **FliptR** molecules are partially planarized in the membrane. **b**–**d**, With increasing tension, three structural changes could occur: a loosening of the packing with increasing distance between less ordered lipid acyl chains, leading to **FliptR** deplanarization (**b**), a tilting and stretching of more ordered acyl chains, which should lead to more compression of the **FliptR** probe and thus planarization (**c**), and phase separation, in which case, **FliptR** molecules are more planarized in the L_o phase and less planarized in the L_d phase (**d**).

(Supplementary Fig. 4). We thus concluded that **FliptR** is insensitive to membrane polarization.

The last possibility to explain the coupled changes in lifetime and tension was that tension changes induce phase separation (Fig. 4d). Recent studies have shown that changes in tension can cause a lipid phase separation to accommodate the area change[46–51]. In such a case, while the membrane is initially homogeneous, domains appear on increasing the membrane tension. The newly formed L_d phase supports most of the stretch, while L_o domains cluster the lipids that cannot be stretched easily. To test this possibility, GUVs were prepared with a lipid composition (DOPC:SM:CL 1:1:1) that mimics the phase separation state of cell membranes by being close to the transition from L_d to mixed L_d–L_o phases[52], and thus more prone to phase separate on applying tension. These GUVs were aspirated into a micropipette to increase their tension (Fig. 5a). As expected, the formation of large domains (visualized through the lifetime image of **FliptR**, see also Fig. 1c) could be observed reproducibly in GUVs aspirated in micropipettes after an abrupt increase in aspiration (Fig. 5c). Moreover, following aspiration, while the lifetime increased in the L_o domains and decreased in the L_d domains, the average lifetime of **FliptR** on the entire GUV increased following aspiration (Fig. 5c, middle and right panels). This shows that the **FliptR** lifetime increase with a membrane tension increase in cells (Fig. 3d) can be attributed to increased lipid phase separation. To further support this hypothesis, we directly investigated changes in the homogeneity of the membrane **FliptR** lifetime under hypertonic shocks. At rest, the **FliptR** lifetime image showed areas of higher lifetime (Fig. 5d and Supplementary Video 2), which are probably related to inhomogeneities of the lipid composition. After a hypertonic shock, these areas seemed to disappear (Fig. 5d and Supplementary Video 2), suggesting that, with a membrane tension decrease, the local plasma membrane composition becomes more homogeneous.

Thus, the **FliptR** response to tension in cells strongly depends on a tension-induced change in phase separation, a mechanism that explains the overall change of **FliptR** lifetime in response to osmotic shocks in cells. Following tension-induced phase separation, the overall lifetime response is dominated by **FliptR** in the more ordered phase (Fig. 4a, d). This explanation seems reasonable considering the almost equal partitioning of **FliptR** into L_d and L_o phases[33], but larger area of L_o phase compared to L_d, resulting from tension-induced phase separation (Fig. 5c)[46,47]. Moreover, the absorptivity of the **FliptR** probe in the L_o phase is higher than in the L_d phase at the excitation wavelength (485 nm)[2]. Thus, the contribution to the overall lifetime counts in FLIM histograms from **FliptR** molecules in the L_o phase is larger than from those in the L_d phase, as seen from the increased photon counts when phase separated (Fig. 5c). Similarly, the decreasing **FliptR** lifetime with decreasing tension under hyperosmotic stress is explained by a reduction of the phase separation, most probably because of partial mixing of the L_o–L_d phases[48,49].

Conclusion

We have reported the use of **FliptR** as a fluorescent probe that allows reliable imaging of membrane tension in living cells and model membranes by FLIM. The intrinsic dependence of the **FliptR** response on lipid composition naturally prevents the attribution of absolute values of **FliptR** lifetime to membrane tension that would be valid for all cells. We provide here calibration curves available to other users for two of the most commonly used cell lines, MDCK and HeLa cells (Fig. 3d).

Increasing lifetimes with increasing tension show that **FliptR** planarizes with an increase in tension. This response is consistent with tension-induced lipid phase separation into more ordered domains with more planarized probes and less ordered domains with more deplanarized probes. These tension-induced domains have been observed previously in model membranes with other techniques[46–51]. In cells, the size of the tension-induced microdomains is probably below detection limits, and they might move too quickly for FLIM imaging. However, the observed overall increase in lifetime with increased membrane tension is consistent with tension-induced domain formation, as in GUVs.

FliptR deplanarization due to lowering of lipid packing by tension is observed in ordered membrane phases that do not phase separate in our experimental conditions. The typical value of this response (Fig. 5b, -1.32 to -0.27 ns m mN^{-1}) is in the range of the response due to phase separation (Fig. 3d, 0.57–2.38 ns m mN^{-1}). However, in cells, the contribution of the effects may be very different in hypo- and hyperosmotic conditions: in hypoosmotic conditions, the overall change in lifetime was fairly small, whereas dramatic changes in lifetime were observed for hyperosmotic conditions (Fig. 3b,d). This could be explained by the fact that in hypoosmotic shocks, both changes in lipid packing (Figs. 4b and 5b) and phase separation (Figs. 4d and 5c) contribute to changes in lifetime. As the two effects have opposite contributions, but of the same order of magnitude, they cancel one another, so the overall response is negligible. Under hyperosmotic conditions, however, the lipids relax to their most compressed state, even for small hyperosmotic shocks. In this case, only changes in phase separation could thus act on **FliptR**, leading to larger changes in the lifetime with

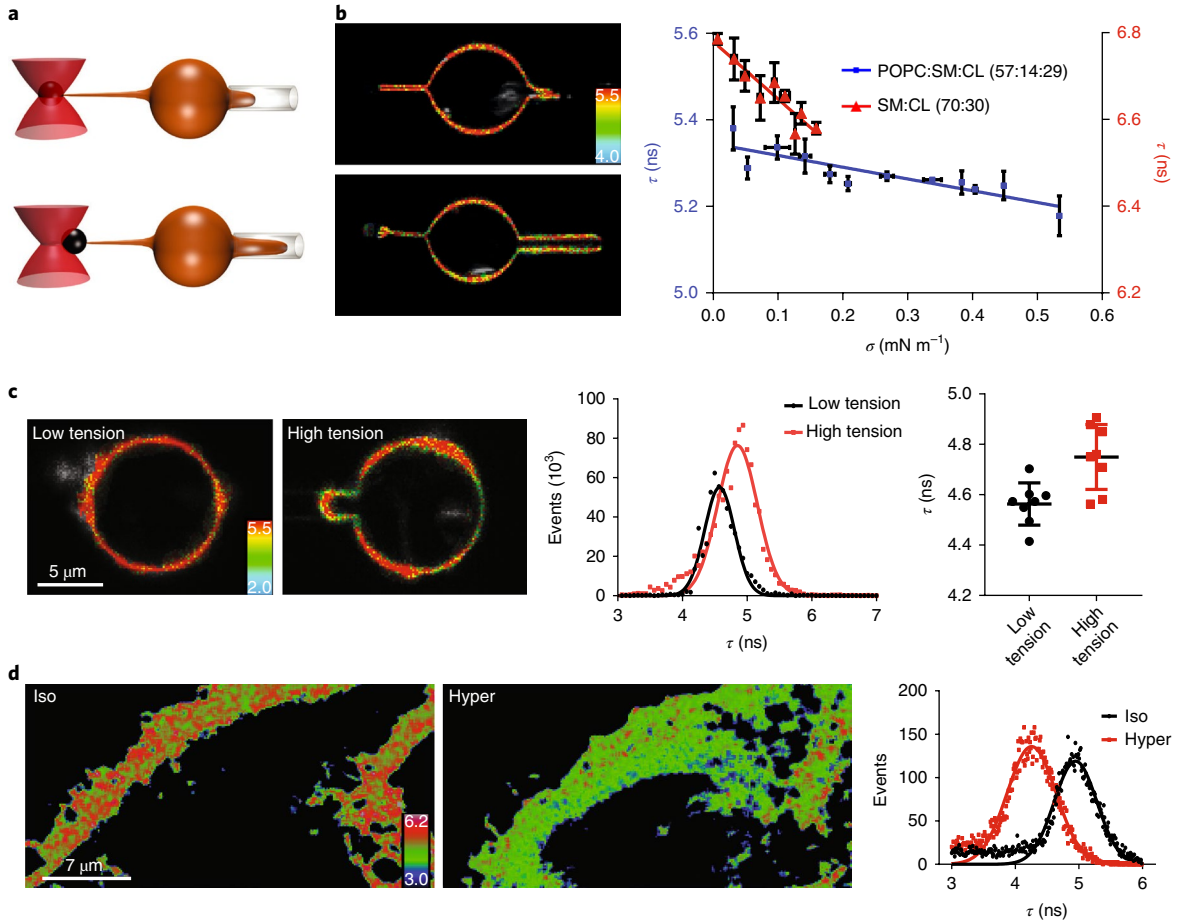

Fig. 5 | Response of FliptR lifetime to membrane tension in GUVs with and without phase separation induced by micropipette aspiration. a, Schematics of the micropipette tube pulling assay. **b**, FLIM images and dependence of lifetimes τ_1 on membrane tension σ for SM/CL 70:30 (red triangles, slope = −1.32 ± 0.19 ns m mN^{-1}, N = 6 GUVs) and POPC:SM:CL 57:14:29 (blue squares, slope = −0.27 ± 0.05 ns m mN^{-1}, N = 7 GUVs). **c**, Left: FLIM images of DOPC:SM:CL 30:30:40 GUVs aspirated in micropipettes and undergoing phase separation at high tension. Middle: Distribution of fluorescence lifetimes with Gaussian fits at low tension (black) and high tension (red). Right: Average lifetimes (N = 8 GUVs) for GUVs at low tension (black) and high tension (red). Centre lines and error bars are mean ± s.d. **d**, Left: Lifetime images of the membrane (confocal image of the lamellipodium) of a HeLa cell under isoomosmotic conditions (Iso) and after hyperosmotic shock (Hyper). Right: Corresponding lifetime histograms (N = 3). The colour bar code corresponds to lifetime in ns.

decreasing membrane tension (Fig. 3d). Contributions from lipid tilting and changes in transmembrane voltage from the response of **FliptR** to tension could be excluded.

FliptR offers an ideal combination of characteristics to accurately image membrane tension in live cells. It combines (1) partitioning into different membrane domains without strong preference[33]; (2) negligible disturbance of the structure of the surrounding membrane[36]; (3) specific labelling of the plasma membrane[2]; (4) negligible fluorescence in water[2,53,54]; (5) insensitivity to membrane potential. An intrinsic limitation of **FliptR** is in reporting lipid packing, which depends on the combination of tension and lipid composition. However, it is difficult to imagine a way other than sensing lipid packing to report membrane tension at the molecular level. Thus, the design of a membrane tension probe insensitive to lipid composition is unlikely. Nevertheless, despite this limitation, **FliptR** accurately reports membrane tension changes, which occur on a timescale of a few seconds, which are easily discriminated from lipid composition changes, which occur over tens of minutes.

It is safe to predict that **FliptR** will not remain the only tension probe. Established systems to image changes in membrane order such as molecular rotors[21,23–25,28–30] or solvatochromic probes[23,54,55] could also function as tension probes. However, further development will be required to adapt these molecules to the list of characteristics required to measure membrane tension. For instance, sufficient partitioning into the L_o membranes is difficult to achieve[21,23–25,28–30,56], as these fluorescent probes disturb the local order of lipids. This study is proposed as an example to encourage fluorescent probe experts to elaborate on the compatibility of their systems with the imaging of membrane tension.

The availability of **FliptR** opens new opportunities to study cell membrane processes by offering the unique possibility to directly image membrane tension in living cells. We foresee new possibilities in studying the role of membrane tension during cell division, endocytosis or cell migration. Preliminary studies focusing on the activation of TORC2 signalling by membrane tension in yeast cells fully support these high expectations, including corroborative evidence for tension-induced phase separation[57]. Moreover, the future design of flipper probes localizing specifically to organelles will enable the community to study intracellular membrane tension, as well as its regulation. Finally, in tissue cells, membrane tension may be a direct reporter of force fields existing in growing tissues. Further studies will determine if the **FliptR** probe can prove itself a direct way to measure those force fields during development.

Methods

FliptR synthesis. FliptR probes were synthesized following reported procedures[30]. Analytical data for the final product are identical to reported data and thus consistent with the structure and purity of the mechanophore.

GUVs preparation and lifetime imaging. GUVs were prepared by the electroformation technique. All lipids were purchased from Avanti Polar Lipids. The lipid solutions used (2 mg ml^{-1}) were (1) pure 1,2-dioleoyl-*sn*-glycero-3-phosphocholine (DOPC), (2) a mixture of DOPC 70 mol% and cholesterol 30 mol%, (3) *N*-(dodecanoyl)-sphing-4-enine-1-phosphocholine (brain sphingomyelin) 58 mol%, DOPC 25 mol%, cholesterol 17 mol%, (4) 70 mol% brain sphingomyelin and 30 mol% of cholesterol, and finally (5) 1-palmitoyl-2-oleoyl-*sn*-glycero-3-phosphocholine (POPC) 80 mol%, sphingomyelin 18.97 mol% and cholesterol 40 mol%. Each lipid solution on $CHCl_3$ was supplemented with **FliptR** (from DMSO solution) at 1 mol% and 0.03 mol% DSPE-PEG2000-biotin.

The lipid solution was spread on indium tin oxide (ITO)-coated glass slides, previously cleaned with bi-distilled water, EtOH and $CHCl_3$. The ITO slides with the lipid was dried by keeping the slides at 30 °C for 2 h. The chamber was assembled using O-ring as spacer, filled with a 297 mOsm sucrose solution and blocked with silicone elastomer. An electric field (10 Hz, 1.1 V) was then applied for 2 h at 55 °C for sphingomyelin-containing lipid mixes or at room temperature otherwise.

Lifetime imaging was carried out in a flow chamber, as described for osmotic shocks on cells. Before addition of the GUV solution, the coverslip was incubated with avidin (from egg white, Life Technologies, 434401) at 0.1 mg ml^{-1} for 10 min. The avidin was washed out three times with ddH_2O, and the flow chamber was filled with 200 µl of PBS. GUVs (5 µl) were then flushed in the flow chamber. Once the GUVs started to partially adhere to the surface, to avoid further adhesion, which could lead to GUV bursting, the remaining glass-bound avidin was blocked by flowing BSA–biotin (1 mg ml^{-1}, Sigma-Aldrich, A8549) for 15 min.

Lifetime measurements. FLIM imaging was performed using a Nikon Eclipse Ti A1R microscope equipped with a time-correlated single-photon counting module from PicoQuant[58]. Excitation was performed using a pulsed 485 nm laser (PicoQuant, LDH-D-C-485) operating at 20 MHz, and the emission signal was collected through a 600/50 nm bandpass filter using a gated PMA hybrid 40 detector and a TimeHarp 260 PICO board (PicoQuant). SymPhoTime 64 software (PicoQuant) was then used to fit fluorescence decay data (from full images or regions of interest) to a dual exponential model after deconvolution for the instrument response function (measured using the backscattered emission light of a 1 µM fluorescein solution with 4 M KI). Data were expressed as means ± s.d. of the mean. The full-width at half-maximum response of the instrument was measured at 176 ps.

Supplementary Fig. 1a shows all parameters extracted from the fits of **FliptR** in various GUV compositions. As similar tendencies were seen for τ_1 and τ_2, the longest lifetime (τ_1), obtained by double exponential fits, was used for all subsequent graphs.

Optical tweezers tube pulling experiment. Tube pulling tension measurements were performed using a modified version of a published set-up[15], which allowed simultaneous bright-field and FLIM imaging on an inverted Nikon Eclipse Ti A1R microscope. A membrane nanotube was formed by pulling away a micropipette-aspirated GUV, whose membrane was attached to a streptavidin-coated bead (3.05 mm diameter, Spherotec) held in a fixed optical trap. The trap was obtained by focusing an ytterbium fibre laser (IPG laser) through a ×100, 1.3 NA oil immersion objective (Nikon). Force measurements were carried out by measuring the displacement of the bead in the optical trap with a C-MOS camera (Pixelink) with a home-made video recorder and bead tracking software under Matlab. The force F exerted on the bead was calculated from Hooke's law: $F = k\,\Delta x$, where k is the stiffness of the trap ($k = 8.58$ pN pix^{-1} W^{-1}) and Δx is the displacement of the bead from its initial zero-force position.

Data processing. Images were analysed and processed with SymPho Time64 and ImageJ. All graphs were constructed with GraphPad Prism 7. Blender software was used for drawings.

Reporting Summary. Further information on experimental design is available in the Nature Research Reporting Summary linked to this article.

Data availability. The data sets generated during the current study are available from the corresponding author upon reasonable request.

Received: 22 December 2017; Accepted: 25 July 2018;
Published online: 27 August 2018

References

1. Helfrich, W. Elastic properties of lipid bilayers: theory and possible experiments. *Zur Naturforschung C* **28**, 693–703 (1973).
2. Soleimanpour, S. et al. Headgroup engineering in mechanosensitive membrane probes. *Chem. Commun.* **52**, 14450–14453 (2016).
3. Evans, E., Heinrich, V., Ludwig, F. & Rawicz, W. Dynamic tension spectroscopy and strength of biomembranes. *Biophys. J.* **85**, 2342–2350 (2003).
4. Rawicz, W., Smith, B. A., McIntosh, T. J., Simon, S. A. & Evans, E. Elasticity, strength, and water permeability of bilayers that contain raft microdomain-forming lipids. *Biophys. J.* **94**, 4725–4736 (2008).
5. Lieber, A. D., Schweitzer, Y., Kozlov, M. M. & Keren, K. Front-to-rear membrane tension gradient in rapidly moving cells. *Biophys. J.* **108**, 1599–1603 (2015).
6. Lieber, A. D., Yehudai-Resheff, S., Barnhart, E. L., Theriot, J. A. & Keren, K. Membrane tension in rapidly moving cells is determined by cytoskeletal forces. *Curr. Biol.* **23**, 1409–1417 (2013).
7. Pontes, B. et al. Membrane tension controls adhesion positioning at the leading edge of cells. *J. Cell Biol.* **216**, 2957–2977 (2017).
8. Gauthier, N. C., Masters, T. A. & Sheetz, M. P. Mechanical feedback between membrane tension and dynamics. *Trends. Cell Biol.* **22**, 527–535 (2012).
9. Gauthier, N. C., Fardin, M. A., Roca-Cusachs, P. & Sheetz, M. P. Temporary increase in plasma membrane tension coordinates the activation of exocytosis and contraction during cell spreading. *Proc. Natl Acad. Sci. USA* **108**, 14467–14472 (2011).
10. Masters, T. A., Pontes, B., Viasnoff, V., Li, Y. & Gauthier, N. C. Plasma membrane tension orchestrates membrane trafficking, cytoskeletal remodeling, and biochemical signaling during phagocytosis. *Proc. Natl Acad. Sci. USA* **110**, 11875–11880 (2013).
11. Sedzinski, J. et al. Polar actomyosin contractility destabilizes the position of the cytokinetic furrow. *Nature* **476**, 462–466 (2011).
12. Lafaurie-Janvore, J. et al. ESCRT-III assembly and cytokinetic abscission are induced by tension release in the intercellular bridge. *Science* **339**, 1625–1629 (2013).
13. Boulant, S., Kural, C., Zeeh, J. C., Ubelmann, F. & Kirchhausen, T. Actin dynamics counteract membrane tension during clathrin-mediated endocytosis. *Nat. Cell Biol.* **13**, 1124–1131 (2011).
14. Saleem, M. et al. A balance between membrane elasticity and polymerization energy sets the shape of spherical clathrin coats. *Nat. Commun.* **6**, 6249 (2015).
15. Morlot, S. et al. Membrane shape at the edge of the dynamin helix sets location and duration of the fission reaction. *Cell* **151**, 619–629 (2012).
16. Wang, Y. et al. Single molecule FRET reveals pore size and opening mechanism of a mechano-sensitive ion channel. *eLife* **3**, e01834 (2014).
17. Berchtold, D. et al. Plasma membrane stress induces relocalization of Slm proteins and activation of TORC2 to promote sphingolipid synthesis. *Nat. Cell Biol.* **14**, 542–547 (2012).
18. Sinha, B. et al. Cells respond to mechanical stress by rapid disassembly of caveolae. *Cell* **144**, 402–413 (2011).
19. Gabella, C. et al. Contact angle at the leading edge controls cell protrusion rate. *Curr. Biol.* **24**, 1126–1132 (2014).
20. Warshaviak, D. T., Muellner, M. J. & Chachisvilis, M. Effect of membrane tension on the electric field and dipole potential of lipid bilayer membrane. *Biochim. Biophys. Acta Biomembranes* **1808**, 2608–2617 (2011).
21. Zhang, Y.-L., Frangos, J. A. & Chachisvilis, M. Laurdan fluorescence senses mechanical strain in the lipid bilayer membrane. *Biochem. Biophys. Res. Commun.* **347**, 838–841 (2006).
22. Templer, R. H., Castle, S. J., Rachael Curran, A., Rumbles, G. & Klug, D. R. Sensing isothermal changes in the lateral pressure in model membranes using di-pyrenyl phosphatidylcholine. *Faraday Discuss.* **111**, 41–53 (1999).
23. Haidekker, M. A. & Theodorakis, E. A. Ratiometric mechanosensitive fluorescent dyes: design and applications. *J. Mat. Chem. C* **4**, 2707–2718 (2016).
24. Kuimova, M. K. et al. Imaging intracellular viscosity of a single cell during photoinduced cell death. *Nat. Chem.* **1**, 69–73 (2009).
25. Vysniauskas, A., Balaz, M., Anderson, H. L. & Kuimova, M. K. Dual mode quantitative imaging of microscopic viscosity using a conjugated porphyrin dimer. *Phys. Chem. Chem. Phys.* **17**, 7548–7554 (2015).
26. Kulkarni, R. U. & Miller, E. W. Voltage imaging: pitfalls and potential. *Biochemistry* **56**, 5171–5177 (2017).
27. M'Baye, G., Mély, Y., Duportail, G. & Klymchenko, A. S. Liquid ordered and gel phases of lipid bilayers: fluorescent probes reveal close fluidity but different hydration. *Biophys. J.* **95**, 1217–1225 (2008).
28. Klymchenko, A. S. Solvatochromic and fluorogenic dyes as environment-sensitive probes: design and biological applications. *Acc. Chem. Res.* **50**, 366–375 (2017).
29. Su, D., Teoh, C. L., Wang, L., Liu, X. & Chang, Y.-T. Motion-induced change in emission (MICE) for developing fluorescent probes. *Chem. Soc. Rev.* **46**, 4833–4844 (2017).
30. Sherin, P. S. et al. Visualising the membrane viscosity of porcine eye lens cells using molecular rotors. *Chem. Sci.* **8**, 3523–3528 (2017).
31. Vyšniauskas, A. et al. Tuning the sensitivity of fluorescent porphyrin dimers to viscosity and temperature. *Chem. Eur. J.* **23**, 11001–11010 (2017).

32. Fin, A., Vargas Jentzsch, A., Sakai, N. & Matile, S. Oligothiophene amphiphiles as planarizable and polarizable fluorescent membrane probes. *Angew. Chem. Int. Ed.* **51**, 12736–12739 (2012).
33. Dal Molin, M. et al. Fluorescent flippers for mechanosensitive membrane probes. *J. Am. Chem. Soc.* **137**, 568–571 (2015).
34. Rawicz, W., Olbrich, K. C., McIntosh, T., Needham, D. & Evans, E. Effect of chain length and unsaturation on elasticity of lipid bilayers. *Biophys. J.* **79**, 328–339 (2000).
35. Verolet, Q. et al. Twisted push–pull probes with turn-on sulfide donors. *Helv. Chim. Acta* **100**, 11564 (2017).
36. Neuhaus, F. et al. Correlation of surface pressure and hue of planarizable push–pull chromophores at the air/water interface. *Beilstein J. Org. Chem.* **13**, 1099–1105 (2017).
37. Sampaio, J. L. et al. Membrane lipidome of an epithelial cell line. *Proc. Natl Acad. Sci. USA* **108**, 1903–1907 (2011).
38. van Meer, G. & Simons, K. Lipid polarity and sorting in epithelial cells. *J. Cell. Biochem.* **36**, 51–58 (1988).
39. Pietuch, A., Brückner, B. R. & Janshoff, A. Membrane tension homeostasis of epithelial cells through surface area regulation in response to osmotic stress. *Biochim. Biophys. Acta* **1833**, 712–722 (2013).
40. Dai, J. W., Sheetz, M. P., Wan, X. D. & Morris, C. E. Membrane tension in swelling and shrinking molluscan neurons. *J. Neurosci.* **18**, 6681–6692 (1998).
41. Alam Shibly, S. U., Ghatak, C., Sayem Karal, M. A., Moniruzzaman, M. & Yamazaki, M. Experimental estimation of membrane tension induced by osmotic pressure. *Biophys. J.* **111**, 2190–2201 (2016).
42. Gauthier, N. C., Rossier, O. M., Mathur, A., Hone, J. C. & Sheetz, M. P. Plasma membrane area increases with spread area by exocytosis of a GPI-anchored protein compartment. *Mol. Biol. Cell.* **20**, 3261–3272 (2009).
43. Ben-Shaul, A. in *Molecular Theory of Chain Packing, Elasticity and Lipid–Protein Interaction in Lipid Bilayers* (eds Lipowsky, R. & Sackmann, E.) Vol. 1, 359–401 (Elsevier, 1995).
44. Mackley, M. Stretching polymer chains. *Rheol. Acta* **49**, 443–458 (2010).
45. Koynova, R. & Caffrey, M. Phases and phase transitions of the phosphatidylcholines. *Biochim. Biophys. Acta Rev. Biomembranes* **1376**, 91–145 (1998).
46. Ho, J. C. S., Rangamani, P., Liedberg, B. & Parikh, A. N. Mixing water, transducing energy, and shaping membranes: autonomously self-regulating giant vesicles. *Langmuir* **32**, 2151–2163 (2016).
47. Oglęcka, K., Rangamani, P., Liedberg, B., Kraut, R. S. & Parikh, A. N. Oscillatory phase separation in giant lipid vesicles induced by transmembrane osmotic differentials. *eLife* **3**, e03695 (2014).
48. Yanagisawa, M., Imai, M. & Taniguchi, T. Shape deformation of ternary vesicles coupled with phase separation. *Phys. Rev. Lett.* **100**, 148102 (2008).
49. Oglęcka, K., Sanborn, J., Parikh, A. N. & Kraut, R. S. Osmotic gradients induce bio-reminiscent morphological transformations in giant unilamellar vesicles. *Front. Physiol.* **3**, 120 (2012).
50. Chen, D. & Santore, M. M. Three dimensional (temperature–tension–composition) phase map of mixed DOPC-DPPC vesicles: two solid phases and a fluid phase coexist on three intersecting planes. *Biochim. Biophys. Acta* **1838**, 2788–2797 (2014).
51. Hamada, T., Kishimoto, Y., Nagasaki, T. & Takagi, M. Lateral phase separation in tense membranes. *Soft Matter* **7**, 9061–9068 (2011).
52. Petruzielo, R. S., Heberle, F. A., Drazba, P., Katsaras, J. & Feigenson, G. W. Phase behavior and domain size in sphingomyelin-containing lipid bilayers. *Biochim. Biophys. Acta* **1828**, 1302–1313 (2013).
53. Macchione, M., Chuard, N., Sakai, N. & Matile, S. Planarizable push–pull probes: overtwisted flipper mechanophores. *ChemPlusChem* **82**, 1062–1066 (2017).
54. Prifti, E. et al. A fluorogenic probe for SNAP-tagged plasma membrane proteins based on the solvatochromic molecule Nile red. *ACS Chem. Biol.* **9**, 606–612 (2014).
55. Mariana, A., Francesco, R., Martin, H., Christian, E. & Erdinc, S. Laurdan and Di-4-ANEPPDHQ probe different properties of the membrane. *J. Phys. D* **50**, 134004 (2017).
56. Doval, D. A. et al. Amphiphilic dynamic NDI and PDI probes: imaging microdomains in giant unilamellar vesicles. *Org. Biomol. Chem.* **10**, 6087–6093 (2012).
57. Riggi, M. et al. A decrease in plasma membrane tension inhibits TORC2 activity via sequestration into PtdIns(4,5)P2-enriched domains. *Nat. Cell Biol.* https://doi.org/10.1038/s41556-018-105-z (in press).
58. Wahl, M., Koberling, F., Patting, M. & Erdmann, H. R. Time-resolved confocal fluorescence imaging and spectrocopy system with single molecule sensitivity and sub-micrometer resolution. *Curr. Pharmaceut. Biotech.* **5**, 299–308 (2004).

Acknowledgements

The authors thank V. Mercier, G. Molinard and M. Laporte for technical support and useful scientific discussions. The authors thank the NMR, MS and Bioimaging platforms for services, and the University of Geneva, the Swiss National Centre of Competence in Research (NCCR) Chemical Biology, the NCCR Molecular Systems Engineering and the Swiss NSF for financial support. A.R. acknowledges funding from the Human Frontier Science Program CDA-0061-08, the Swiss National Fund for Research grants nos. 31003A_130520, 31003A_149975 and 31003A_173087, and the European Research Council Starting Grant no. 311536 (2011 call). E.D. acknowledges funding from Human Frontier Science Program (LT00305/2011-L).

Author Contributions

A.C., N.S., S.M. and A.R. designed the project. S.S. and M.D.M. synthesized the FliptR probe. E.D. and M.G.-G. designed and performed initial FLIM measurements. C.T. developed and made vertical PDMS walls for MDCK cell culture. A.C. performed all other experiments and analysis. A.C., E.D., N.S., S.M. and A.R. wrote the paper.

Competing interests

The authors declare no competing interests.

Additional information

Supplementary information is available for this paper at https://doi.org/10.1038/s41557-018-0127-3.

Reprints and permissions information is available at www.nature.com/reprints.

Correspondence and requests for materials should be addressed to A.R.

Publisher's note: Springer Nature remains neutral with regard to jurisdictional claims in published maps and institutional affiliations.

nature research

Corresponding author(s): Aurélien Roux: Aurelien.roux@unige.ch

Reporting Summary

Nature Research wishes to improve the reproducibility of the work that we publish. This form provides structure for consistency and transparency in reporting. For further information on Nature Research policies, see Authors & Referees and the Editorial Policy Checklist.

Statistical parameters

When statistical analyses are reported, confirm that the following items are present in the relevant location (e.g. figure legend, table legend, main text, or Methods section).

n/a	Confirmed	
☐	☒	The exact sample size (*n*) for each experimental group/condition, given as a discrete number and unit of measurement
☒	☐	An indication of whether measurements were taken from distinct samples or whether the same sample was measured repeatedly
☐	☒	The statistical test(s) used AND whether they are one- or two-sided *Only common tests should be described solely by name; describe more complex techniques in the Methods section.*
☐	☒	A description of all covariates tested
☐	☒	A description of any assumptions or corrections, such as tests of normality and adjustment for multiple comparisons
☐	☒	A full description of the statistics including central tendency (e.g. means) or other basic estimates (e.g. regression coefficient) AND variation (e.g. standard deviation) or associated estimates of uncertainty (e.g. confidence intervals)
☐	☒	For null hypothesis testing, the test statistic (e.g. *F*, *t*, *r*) with confidence intervals, effect sizes, degrees of freedom and *P* value noted *Give P values as exact values whenever suitable.*
☐	☒	For Bayesian analysis, information on the choice of priors and Markov chain Monte Carlo settings
☐	☒	For hierarchical and complex designs, identification of the appropriate level for tests and full reporting of outcomes
☐	☒	Estimates of effect sizes (e.g. Cohen's *d*, Pearson's *r*), indicating how they were calculated
☐	☒	Clearly defined error bars *State explicitly what error bars represent (e.g. SD, SE, CI)*

Our web collection on statistics for biologists may be useful.

Software and code

Policy information about availability of computer code

Data collection	SymPhoTime 64
Data analysis	SymPhoTime 64: Fitting the lifetime images. -Excel: Group of data and measurement of median and standard deviation GraphPad Prism: To plot graphs and obtain the linear regression -ImageJ: To extract the histograms of the images

For manuscripts utilizing custom algorithms or software that are central to the research but not yet described in published literature, software must be made available to editors/reviewers upon request. We strongly encourage code deposition in a community repository (e.g. GitHub). See the Nature Research guidelines for submitting code & software for further information.

Data

Policy information about availability of data

All manuscripts must include a data availability statement. This statement should provide the following information, where applicable:

- Accession codes, unique identifiers, or web links for publicly available datasets
- A list of figures that have associated raw data
- A description of any restrictions on data availability

The data sets generated during the current study are available from the corresponding author upon reasonable request.

Field-specific reporting

Please select the best fit for your research. If you are not sure, read the appropriate sections before making your selection.

☒ Life sciences ☐ Behavioural & social sciences ☐ Ecological, evolutionary & environmental sciences

For a reference copy of the document with all sections, see nature.com/authors/policies/ReportingSummary-flat.pdf

Life sciences study design

All studies must disclose on these points even when the disclosure is negative.

Sample size	The error bars and the measure of the center is mean ± SD. In each measurement was taken several GUV's and cells giving an important number of events, together with the small differences between replications were the indication of the sample size for each experiment Lifetime vs lipid composition(GUV) (fig 1c and Suppl fig a) DOPC-- R:15 DOPC:CL-- R:25 Phase separated-- R:5 SM:CL-- R:25 Lifetime vs osmotic pressure (fig 3b): GUV-- R:85 MDCK-- R:20 HeLa-- R:22 Lifetime vs osmotic shocks (fig 5d): Hela-- R:3 (Paper one exeample) lifetime vs tension (fig 3d): MDCK-- R:11 HeLa-- R:7 Lifetime vs tension (GUVs) (fig 5): GUV (POPC:SM:CL)-- R:7 GUV (SM:CL)-- R:6 GUV (DOPC:SM:CL)-- R:8 lifetime vs time during osmotic shocks: GUVs (DOPC) : R:14 (suppl fig 3a) GUVs (POPC:SM:CL) : R: 6 (suppl fig 3b) Hela (control w/o shock): R:21 (suppl fig 2a) MDCK (control w/o shock):R:19 (suppl fig 2a) Hela : R:14 (suppl fig 2b) MDCK :R:49 (suppl fig 2b)
Data exclusions	Not relevant
Replication	Lifetime vs lipid composition(GUV) (fig 1c and Suppl fig a) DOPC-- N:5 DOPC:CL-- N:5 Phase separated-- N:4 SM:CL-- N:5 Lifetime vs osmotic pressure (fig 3b): GUV-- N:4 MDCK-- N:6 HeLa-- N:20

lifetime vs tension (fig 3d):
MDCK-- N:11
HeLa-- N:7

Lifetime vs osmotic shocks (fig 5d):
Hela-- N:3 (Paper one exeample)

Lifetime vs tension (GUVs, fig 5) :
GUV (POPC:SM:CL)-- N:7
GUV (SM:CL)-- N:6
GUV (DOPC:SM:CL)-- N:8

lifetime vs time during osmotic shocks:
GUVs (DOPC) : N:2 (suppl fig 3a)
GUVs (POPC:SM:CL) : N:1 (suppl fig 3b)
Hela (control w/o shock): N:2 (suppl fig 2a)
MDCK (control w/o shock):N:2 (suppl fig 2a)
Hela : N:2 (suppl fig 2b)
MDCK :N:2 (suppl fig 2b)

Neurons--KCl and Osmotic shock (suppl fig 4): N:3

Randomization: Not relevant

Blinding: Not relevant

Reporting for specific materials, systems and methods

Materials & experimental systems

n/a	Involved in the study
☒	☐ Unique biological materials
☒	☐ Antibodies
☐	☒ Eukaryotic cell lines
☒	☐ Palaeontology
☒	☐ Animals and other organisms
☒	☐ Human research participants

Methods

n/a	Involved in the study
☒	☐ ChIP-seq
☒	☐ Flow cytometry
☒	☐ MRI-based neuroimaging

Eukaryotic cell lines

Policy information about cell lines

Cell line source(s): HeLa-Zerial cell line, obtained from Lukas Pelkmans published in: Pelkmans L et al. Genome-wide analysis of human kinases in clathrin- and caveolae/raft-mediated endocytosis. Nature. 2005 Jul 7;436(7047):78-86.

MDCK-II cells: bought from Sigma-Aldrich, Ref: 00062107, from Public Health England

Authentication: by the providers

Mycoplasma contamination: cells lines are tested every 6 months for mycoplasma contamination. These cells lines were tested before use for these experiments and was negative.

Commonly misidentified lines (See ICLAC register): Not misidentified lines were used